Extensions of the Chalmers Nonlinear HEMT and MESFET Model

Iltcho Angelov, *Member, IEEE*, Lars Bengtsson, *Student Member, IEEE*, and Mikael Garcia, *Student Member, IEEE*

***Abstract*— The ability to simulate temperature, dispersion, and soft-breakdown effects as well as a new α dependence was added to the Chalmers nonlinear model for high electron mobility transistor (HEMT's) and metal semiconductor field-effect transistor (MESFET's). DC, pulsed dc, low frequency (10 Hz–10 MHz), RF, and small signal S-parameter measurements (1–18 GHz) have been made on a large number of commercial HEMT and MESFET devices from different manufacturers in the temperature range 17–400 K in order to evaluate the validity of the model extensions.**

I. Introduction

IN THE DESIGN of nonlinear active circuits, harmonic balance simulations or Volterra series analyzes are very useful. As the computers running the CAD programs are becoming more and more powerful and the high precision measurement instruments are getting less expensive, the need for accurate device models for high precision simulations is growing. In the field of nonlinear modeling of high electron mobility transistor (HEMT's) and metal semiconductor field-effect transistor (MESFET's) different models have been presented during the past years [1]–[3].

It is well known that a large signal model extracted from experimental dc data does not fully describe the transistors' behavior at RF. For example, there is a discrepancy between the dc and RF transconductance as well as output conductance due to temperature and dispersion effects. A common explanation is that traps and surface states in the semiconductor affect the performance of the device.

These effects should be considered in the design of circuits like power amplifiers, cryogenic amplifiers, etc. [4]–[9]. Better large signal models can be extracted if the dc characteristics are measured by pulsed measurements. If the pulses are kept short the traps will not affect the device characteristics. The pulse period should be shorter than the mean life time of the traps. For cryogenic applications the dc characteristics have to be made at operating temperature to make the extraction of accurate models possible.

Soft breakdown, a non destructive drain current breakdown for high drain voltages, can be observed for some HEMT's and MESFET's. Transistors operating in this region should be modeled in such a way as to take this into account.

Manuscript received August 31, 1995; revised June 14, 1996. This work was supported in part by The Swedish Defence Material Administration (FMV) and The Swedish National Board for Industrial and Technical Development (NUTEK).

The authors are with the Department of Microwave Technology, Chalmers University of Technology, S-41296 Göteborg, Sweden.

Publisher Item Identifier S 0018-9480(96)06902-5.

The purpose of this paper is to extend the Chalmers Model to account for temperature, dispersion and soft break down effects.

II. The Model

The equation for the drain-source current in the Chalmers model is

$$I_{\rm ds} = I_{pk}(1+\tanh(\Psi))\tanh(\alpha V_{\rm ds})(1+\lambda V_{\rm ds}) \quad (1)$$

Ψ is in general a power series function centred at V_{pk} and with a variable $V_{\rm gs}$, i.e.,

$$\Psi = P_1(V_{\rm gs}-V_{pk}) + P_2(V_{\rm gs}-V_{pk})^2 + P_3(V_{\rm gs}-V_{pk})^3 \cdots \quad (2)$$

where I_{pk} is the drain current and V_{pk} the gate voltage at which the maximum of the transconductance occurs, λ is the channel length modulation parameter and α is the saturation voltage parameter [3]. As a first approach we choose P_1 as $P_{1s} = g_{ms}/I_{pks}$, where g_{ms} and I_{pks} are measured in the saturated current region. Since the limit of the function $1+\tanh(\Psi)$ is 2 then I_{pk} should equal or larger than $0.5I_{\max}/(1+\lambda V_{\rm ds})$.

We found that the model worked well using the first term of the function Ψ because P_1 is the only coefficient defining the transconductance value at V_{pk}. If the derivative of the drain current, g_m, is asymmetrical, then 2–3 terms can be added in Ψ. Note that neither P_2 nor P_3 affects the transconductance at V_{pk}. P_2 makes the derivative of the drain current asymmetrical and P_3 changes the drain current values at voltages $V_{\rm gs}$ close to pinch off. Three terms are enough to handle even such complicated devices as described in [10] with linear $I_{\rm ds}$ versus $V_{\rm gs}$ characteristics.

When the device operates in the saturated region, P_1 and V_{pk} can be considered constant. If high accuracy at low drain voltages is important, then the drain voltage dependence of P_1 and V_{pk} should be considered or the values of alternatively P_1 and V_{pk} should be extracted from data measured at the selected bias point. The global behavior of the transistor can be described by the following expressions for V_{pk} and P_1 [11]

$$V_{pk}(V_{\rm ds}) = V_{pk0} + (V_{pks}-V_{pk0})\tanh(\alpha V_{\rm ds}) \quad (3)$$

$$P_1(V_{\rm ds}) = P_{1s}\left[1+\left(\frac{P_{10}}{P_{1s}}-1\right)\frac{1}{\cosh^2(BV_{\rm ds})}\right] \quad (4)$$

where V_{pk0} and V_{pks} are V_{pk} measured at $V_{\rm ds}$ close to zero and in the saturated region, respectively, $P_{10} = g_{mo}/I_{pk0}$ at $V_{\rm ds}$ close to zero and B is a fitting parameter ($B \approx 1.5\alpha$).

We have found for many devices that all coefficients show the same $V_{\rm ds}$ dependence as P_1 thus making it possible to

redefine Ψ as Ψ_1 [12]

$$\Psi_1 = \left[1+\left(\frac{P_{10}}{P_{1s}}-1\right)\frac{1}{\cosh^2(BV_{\rm ds})}\right]\cdot\sum_{l=1}^{\infty} P_{ls}(V_{\rm gs}-V_{pk})^l \quad (5)$$

In the case of large gate and drain voltage swing the coefficient α can not be assumed constant. For MESFET's this dependence is not so strong, but for HEMT's α changes rapidly with the gate voltage and this should be modeled in a proper way. In the approach used by [13], (6), the function α has a pole at gate voltage $V_{\rm gs} = 1/K_g$

$$\alpha = \alpha_0/(1 - K_g V_{\rm gs}) \quad (6)$$

Good correspondence between model and measured results at drain voltages below 1.5 V and at small drain currents $I_{\rm ds}$ as well as much better behavior in the harmonic balance simulation can be reached by using the following expression for α

$$\alpha = \alpha_r + \alpha_1[1 + \tanh(\psi)] \quad (7)$$

where α_1 is constant and α_r is the residual value of α at pinch off. For HEMT's, α_r is usually very small (0.05–0.2). If (7) is used to model α, smaller values of P_3 and P_{10} are achieved. The drain current is greatly influenced at gate voltages close to pinch off due to the use of this type of α dependence. A drawback in using a bias dependent α, is that the extraction process becomes more complex. A good starting point in the extraction process for α and λ is to use the values obtained from the $I_{\rm ds}(V_{\rm ds})$ characteristics at positive gate voltages $V_{\rm gs}$ = 0.2–0.4 V.

III. Measurements and Measurement Set-Up

We made measurements on a number of samples from different commercial MESFET and HEMT device manufacturers[1] in order to investigate how temperature and dispersion effects influence the devices' performance. DC- and S-parameters of the packaged devices were measured in a Maury MT-950 transistor fixture and in a specially developed microstrip fixture that we found suitable in the temperature range 17–400 K. In order to avoid moisture building up during the cool down the transistor fixture was placed in a vacuum box (≈0.001 mBar) and connected to the room temperature part with short (10 cm) stainless steel cables. A Cryogenics Model 350 Refrigerator was used to cool down the transistors and a Lake Shore temperature controller for keeping the temperature stable (within 1 degree) during the measurements. They were usually performed by first cooling down to 17 K and then warming up by using the temperature controller. A TRL calibration was made inside the cool box. A special program was written in LabVIEW in order to make correct calibration, measurements and to store the measured data. A HP4195A VNA was used for measuring low frequency S-parameters (10 Hz–500 MHz) of the transistors and a Wiltron 360B for the measurements in the frequency range 0.1–18 GHz. The equivalent circuit of the transistor shown in Fig. 1 was used to model the packaged transistors. The parasitic parameters L_g, L_d, L_s, C_p etc. were fixed at the values extracted from the S-parameter measurements at $V_{\rm ds}$ = 0 V at room temperature. R_g, R_d, R_s were extracted from dc and cold FET S-parameter measurements as a function of the temperature [14]. The component values of the cold FET small signal equivalent circuit were extracted by using our own extraction program MILOU for Macintosh, but similar results were obtained with MDS (Hewlett-Packard), Scout, and Microwave Harmonica (Compact Software).

[1] NEC32684 (NEC), FHX15FA (Fujitsu), MGF4317D, MGF1404 and, MGF1303B (Mitsubishi) named NEC3, FHX15, MGF4, MGF14, and MGF3, respectively. The first three devices are HEMT's and the last two are MESFET's.

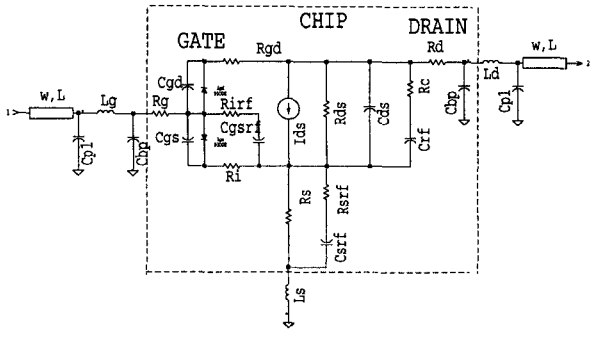

Fig. 1. Equivalent circuit of the HEMT.

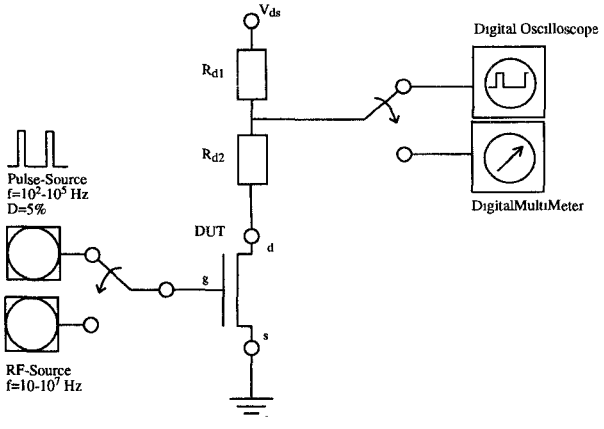

Fig. 2. Block diagram of the dispersion measurement set-up.

Pulsed dc, RF lower region (10 Hz–10 MHz) and S-parameter measurements were performed to find the frequency dispersion of the transconductance and the output conductance of the device [4]–[8], [15]–[17]. DC-parameters were measured by using a HP 4145B parameter analyzer. The block diagram of the pulsed and RF set up is shown in Fig. 2. The devices are usually pulsed for a short period (1 μs) into the active region and are then held in the passive (cut-off) region for the rest of the period (typically 1 ms). In our dc measurement set up with HP4145B a 5 second pause was used between each measured trace in order to allow cooling of the device between the sweeps. The device's transfer characteristic dispersion is influenced both by the output conductance and the transconductance dispersion. A simple way to monitor the dispersion of g_m only is to use resistors with small resistance values (R_{d1} = 2 Ω, R_{d2} = 0 Ω). The connection is working as a current probe. In this case the gain of the circuit A_v is

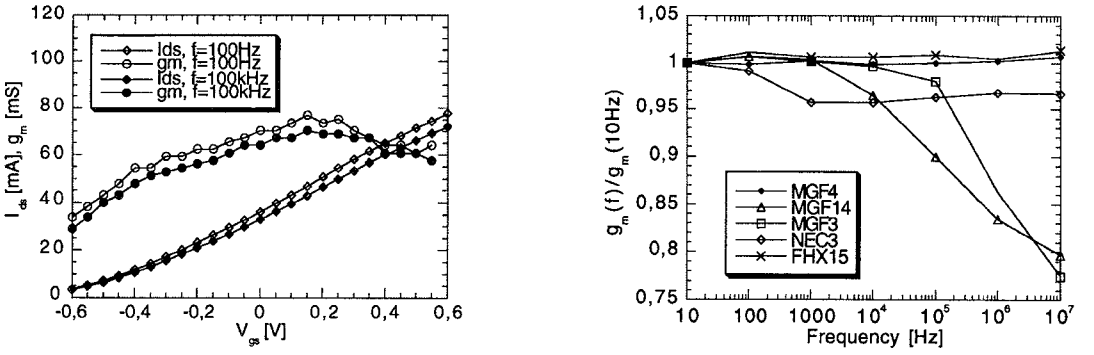

(a) (b)

Fig. 3. (a) Dispersion for MGF1404 from pulsed measurements (b) Dispersion in the peak value of g_m from RF measurements.

given by

$$A_v = g_m \frac{R_{\rm ds} R_{d1}}{R_{\rm ds} + R_{d1}} \approx g_m R_{d1} \tag{8}$$

and the output conductance dispersion will not influence the accuracy of the g_m measurement.

Temperature and self heating effects were studied by using pulsed bias with larger values of the resistances ($R_{d2} = 47\ \Omega$, $R_{d1} = 10\ \Omega$) in order to prevent instabilities and to decouple the transistor from the measuring equipment.

IV. Dispersion Modeling

In Fig. 3(a) and (b) measured frequency dependencies of $I_{\rm ds}$ and g_m extracted from dc, pulsed, and RF measurements are presented. The measured difference between the dc transconductance and the transconductance values, extracted from pulsed dc, RF and S-parameters was small (about 5–10%) for most of the new HEMT devices. We noticed a small increase of the transconductance (2–4%) at high frequencies in some devices compared with the dc value (FHX15, MGF4317D). For the MESFET devices we measured we found that the RF value was always lower than the dc value and that there were some devices for which the dispersion effects were quite substantial, i.e., MGF1404 (a decrease of nearly 25%), Fig. 3(b).

Two approaches were used in modeling the device dispersion: analytical, in which the dispersion phenomenon is incorporated into the equation for the drain current in the large signal model and an approach, where the equivalent circuit is extended with components that model the dispersion effect. The two approaches have both advantages and disadvantages. The equivalent circuit approach is simpler, since it is easy to incorporate it into HB simulators, but not so accurate as the analytical approach.

At operating frequency much lower than one divided by the trapping time constant (typically in the millisecond range), the transconductance, $g_m(\omega)$, and the channel conductance, $G_{\rm ds}(\omega)$, equal the dc value. At high frequencies, when the traps are frozen, the transconductance and the channel conductance reach their RF values. Using the formulation in [15], [17] the drain current consists of three parts

$$\begin{aligned} I_{\rm ds,RF}[V_{\rm gs}(t), V_{\rm ds}(t)] &= I_{\rm ds,dc}[V_{\rm gs}(t), V_{\rm ds}(t)] \\ &+ \Delta I_{\rm ds}[V_{\rm gs}(t), V_{\rm ds}(t)] \\ &+ \Delta \bar{I}_{\rm ds}[V_{\rm gs}(t), V_{\rm ds}(t)] \end{aligned} \tag{9}$$

The first term is the quasistatic I-V characteristics of an ideal dispersionless device. The extra terms are the contributions from the instantaneous transconductance and channel conductance dispersion. This type of $I_{\rm ds,RF}$ dependence can be modeled with a frequency dependent factor, P_{1d}

$$P_1 = P_{1d} P_{1s} \left[1 + \left(\frac{P_{10}}{P_{1s}} - 1 \right) \frac{1}{\cosh^2(B V_{\rm ds})} \right]. \tag{10}$$

The dispersion effects of the g_m can be taken into account by using the frequency dependence proposed in [4]

$$g_m(f) \propto \frac{1}{1 + (f/f_{\rm tr})^2}. \tag{11}$$

This can be incorporated in the model as

$$P_{1d} = \frac{P_{1\rm srf}}{P_{1\rm sdc}} + \frac{P_{1\rm sdc} - P_{1\rm srf}}{P_{1\rm sdc}} \frac{1}{1 + (f/f_{\rm tr})^2} \tag{12a}$$

or in the case of g_m influenced by multiple trapping processes with different trapping frequencies $f_{{\rm tr},1}, \ldots, f_{{\rm tr},n}$

$$P_{1d} = \frac{P_{1\rm srf}}{P_{1\rm sdc}} + \frac{P_{1\rm sdc} - P_{1\rm srf}}{P_{1\rm sdc}} \sum_{n=1}^{N} \frac{K_n}{1 + (f/f_{{\rm tr},n})^2}. \tag{12b}$$

It is also possible to use a smoother type of frequency dependencies like

$$P_{1d} = \frac{P_{1\rm srf}}{P_{1\rm sdc}} + \frac{P_{1\rm sdc} - P_{1\rm srf}}{P_{1\rm sdc}} \sum_{n=1}^{N} \frac{K_n}{\cosh(f/f_{{\rm tr},n})^2}. \tag{13}$$

$P_{1\rm sdc}$ is the P_{1s} measured at dc for saturation drain voltages, $P_{1\rm srf}$ is extracted from the RF measurements and $f_{{\rm tr},1}, \ldots f_{{\rm tr},n}$ are the corner frequencies for the dispersion effects. This approach works well in the frequency domain. One way to incorporate this dependence directly into a HB simulator is to treat the dispersion part, P_{1d}, as a constant. Then it is possible to obtain good results in simulating dc

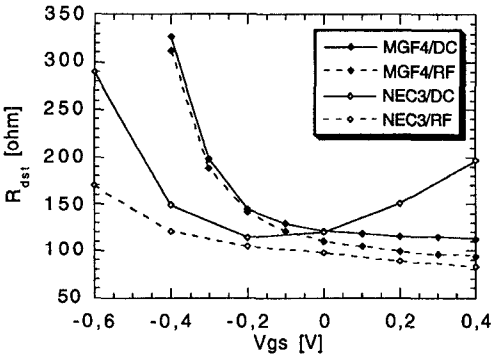

Fig. 4. $R_{\rm ds}$ as function of gate voltage $V_{\rm gs}$ at dc and RF for MGF4317D and NEC32684, $V_{\rm ds} = 2.0$ V.

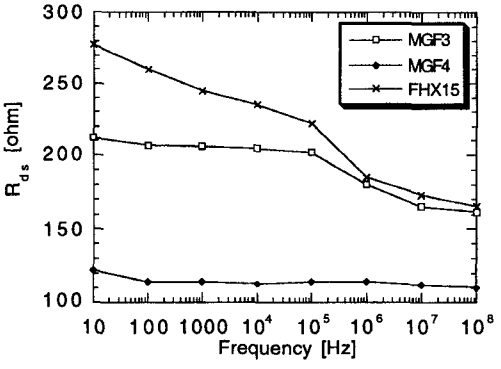

Fig. 5. $R_{\rm ds}$ as function of frequency, $V_{\rm ds} = 2.0$ V, $V_{\rm gs} = 0.0$ V.

and RF performance. Another way is to use a time domain operator, d/dt, in P_{1d} similar to the approach used in [16].

The values of the output resistances $R_{\rm dst} = r_{\rm ch} + R_d + R_s$ were extracted directly from RF data by using an HP 4195A VNA at 100 MHz and an HP 4145B Parameter Analyzer at dc, respectively. In Fig. 4 measured dc data and RF data for two HEMTs, MGF4317D and NEC32684, are shown. The RF values of the output resistance $R_{\rm dst}$ are much lower than the dc values for NEC32684. For other HEMT's, i.e., MGF4317D, the difference between the RF and dc values is much smaller. Explanations for this behavior are given in [4], [7], [8], [18]. We believe that the difference between the RF and dc values of $R_{\rm dst}$ is caused by trapping effects. It is interesting to see that at high positive gate voltages, when the current is large, the dc values of $R_{\rm dst}$ can reach negative values. The reason for this is self heating. The RF output resistance, $R_{\rm dst}$, decreases monotonically with the increase of the gate voltage, as described by the model. Negative $R_{\rm dst}$ is not observed at RF, since in small signal S-parameter measurements the transistor operates under isothermal conditions. Above the gate voltage, at which the dc values of $R_{\rm dst}$ start to increase, pulsed dc measurements should be made because the self heating effects can not be neglected. In Fig. 5 the frequency dependence of the output drain to source resistance $R_{\rm dst}$ is shown. For some transistors, i.e., MGF1303B, there are probably two different trapping processes with different corner frequencies. An RC-series circuit $(R_c, C_{\rm rf})$ was used to model the low frequency dispersion of the output conductance. By

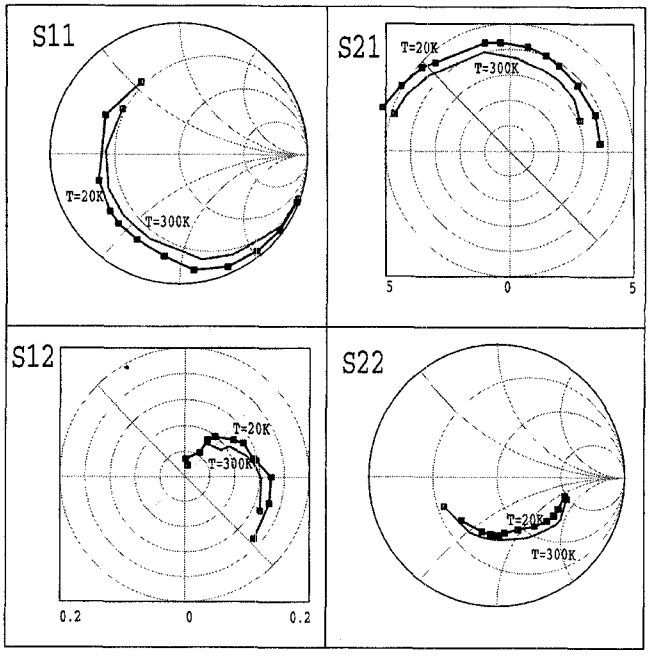

Fig. 6. S-parameters for MGF4317D at 20 and 300 K. Frequency: 1–12 GHz.

adjusting the λ values extracted from the dc measurements and the values of the RC-circuit it was possible to fit simulated to experimental data for both dc characteristics and S-parameters. If the frequency dependence of the output conductance is more complicated and it is important to model this behavior, this can be done by adding an additional RC circuit in parallel with another time constant. A problem arising in using this approach is caused by the fact that in reality R_c is bias dependent. At $V_{\rm gs}$ voltages close to the pinch off, the value of R_c is much higher then the value of R_c under active working conditions. Good correspondence between modeled and measured S-parameters can be reached by using the following expression for gate bias dependence of R_c

$$R_c = R_{c0} + \frac{R_{\rm cpo}}{1 + \tanh(\psi)}$$

where R_{c0} is the minimum value of R_c and $R_{\rm cpo}$ determines the value of R_c at the pinchoff.

A similar approach can be used to model the dispersion of the transconductance [19], [20]. The charging resistance R_i and source parasitic resistance R_s, which in reality are distributed, decrease the value of extrinsic transconductance. This can be modeled by using a dc and an RF part. For HEMT's a noticeable decrease of R_s was reported in the frequency range 1–30 GHz [20], that would lead to an increase of the RF transconductance. We obtained similar results for MGF4317D, FHX15, and other HEMT's. This can be modeled by adding a parallel branch to R_s, R_{srf} and C_{srf}. The time constant of this network should correspond to the dispersion constant of g_m. We have found that a capacitive representation is closer to device physics, especially for HEMT's, because at high frequencies the contact resistance is shunted by the 2DEG depletion capacitance. As R_{sf} is in parallel with R_s,

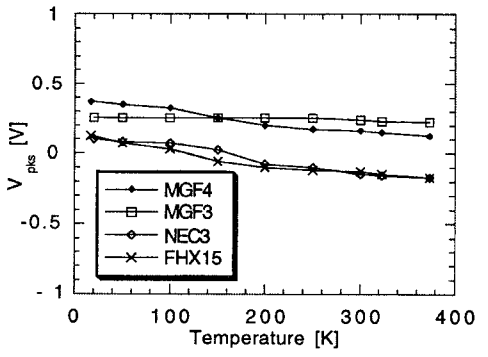

(a)

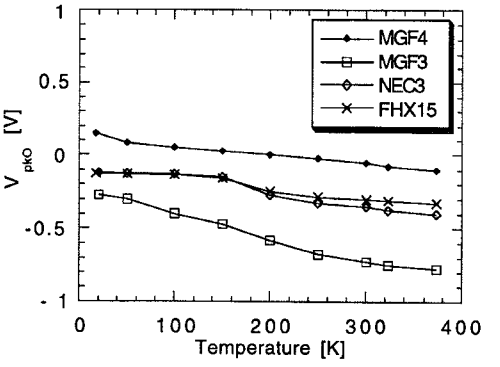

(b)

Fig 7 (a) V_{pks} as function of temperature,(b) V_{pk0} as function of temperature.

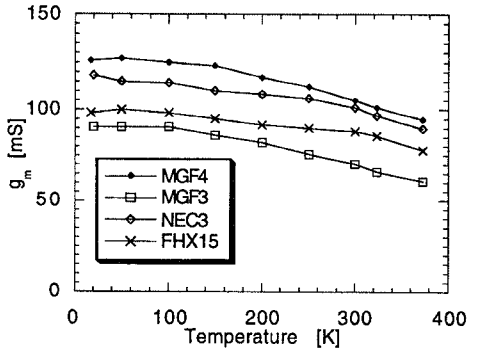

Fig. 8. The peak value of g_m as function of temperature.

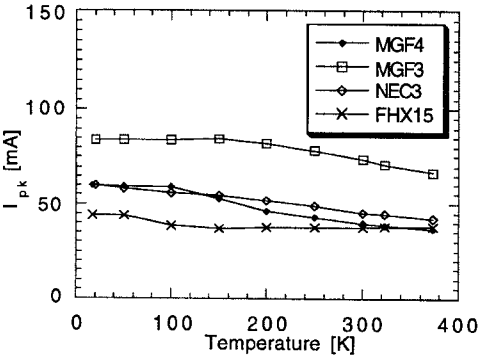

Fig. 9. I_{pk} as function of temperature.

an increase in the transconductance will be obtained at RF. The value of $C_{\rm srf}$ determines the time constant of the process.

The decrease of the transconductance for MESFET's can be described by adding a parallel branch, $R_{\rm rf}$ and $C_{\rm gsrf}$ in series, between the internal gate and source terminals. At frequencies higher than the corner frequencies for the dispersion effects the resistor $R_{\rm rf}$ shunts the input and effectively decreases the transconductance.

The values of I_{pk}, P_{1s}, P_{10}, V_{pk0}, V_{pks}, α, and λ were determined from dc and pulsed dc measurements. A junction model available in the FET model in MDS (HP) was used to model $C_{\rm gs}$, $C_{\rm gd}$ and forward conduction characteristics of the HEMT Schottky diode. The extraction process of the model parameters is described in greater detail in [12]. The most important and critical moment in the parameter extraction is the determination of two main models parameters—I_{pk} and V_{pk}. It is always possible to obtain a good fit for the drain current and first harmonic if you use a value of I_{pk} larger than $I_{\max}/2$. The most common error in the extraction procedure is to perform the measurements with gate voltages not high enough to provide information about the maximum current $I_{\max}$. Other problems are caused by instabilities in the transistor, dispersion, and thermal heating. Together with the noise and errors associated with the measurements this makes the extraction procedure difficult. We have found it useful [11] to make power spectrum measurements (PSM), that can provide information about the parameters of the model (I_{pk} and V_{pk}). Usually the first two harmonics give the necessary information about V_{pk} and I_{pk}—at V_{pk} the second harmonic is at its minimum and the first at its maximum (or close to it).We have also observed that if the measurements are performed at gate voltages high enough to give information about the maximum current, standard fitting programs like Scout and Kaleidagraph can find satisfactory combinations of coefficients.

V. Modeling of the Temperature Dependence

The main parameters of the model—V_{pk0}, V_{pks}, I_{pk}, P_{1s}, P_{10}, λ, $V_{\rm gs}$, R_s, R_d, $C_{\rm gd}$, $C_{\rm gs}$—are also temperature dependent. To evaluate this temperature dependence several transistors from each of the types listed above were measured in the 17–400 K temperature range. The typical measured S-parameters for MGF4317D at two temperatures 20 K and 300 K are presented in Fig. 6. Temperature changes in model parameters for different HEMT and MESFET devices in the temperature range 17–400 K are presented in Figs. 7–13. The voltages at which we have maximum transconductance, V_{pk0} and V_{pks}, increase linearly at low temperatures, Fig. 7. P_{1s} is almost independent of temperature, Fig. 10(a), because of the nearly monotonous increase of both g_m and I_{pk}, Fig. 8, at low temperatures. The changes of the transconductance are mainly due to I_{pks} increase at cryogenic temperatures. The largest change we monitored was the increase of the coefficient P_{10} at cryogenic temperatures, Fig. 10(b). This observation is very important for circuits operating at low drain voltages, such as modulators, resistive mixers, etc. It means that it will

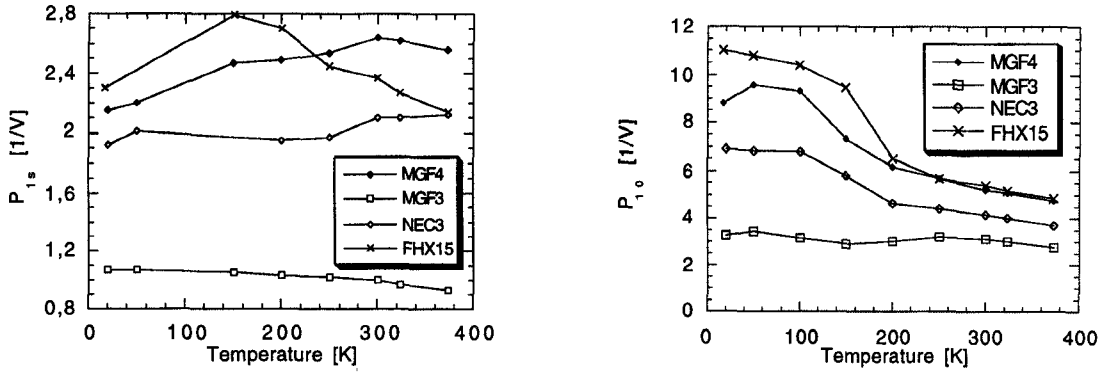

Fig. 10. (a) P_{1s} as function of temperature. (b) P_{10} as function of temperature.

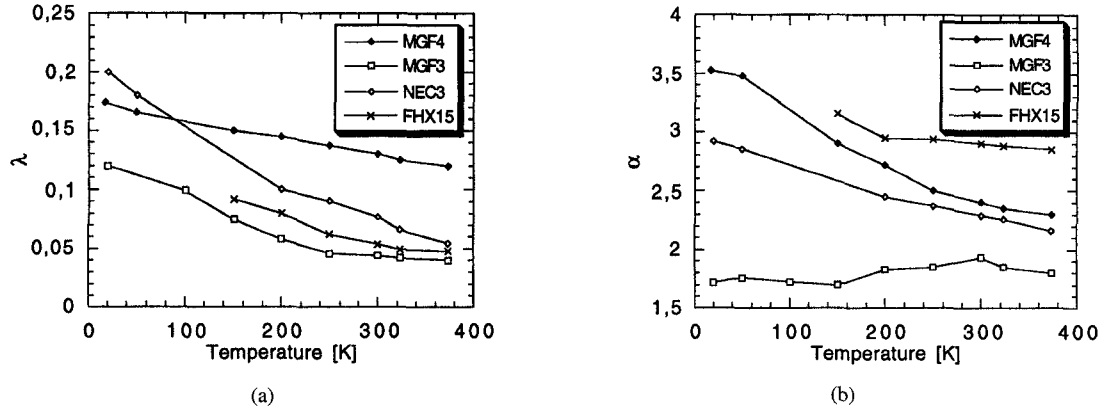

Fig. 11. (a) λ as function of temperature. (b) α as function of temperature.

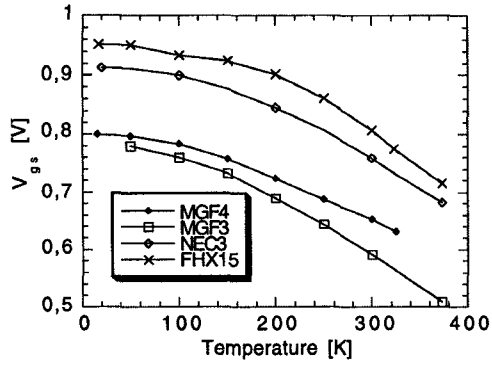

Fig. 12. V_{gs} as function of temperature, $I_{gs} = 0.5$ mA.

be possible to reduce the power that the local oscillator must provide for the full drive of a resistive mixer at cryogenic temperatures. Slight increases of λ and α, Fig. 11(a)–(b), for all transistors are observed at low temperatures.

The forward gate bias voltage at fixed gate current, Fig. 12, increases at cryogenic temperatures. The changes are almost linear in the temperature range 200–400 K and can be used as a thermometer for measuring the channel temperature [18], [21]. At lower temperatures the increase in V_{gs} is not so linear [21].

The source parasitic resistance R_s decreases monotonically at low temperatures, Fig. 13. The changes of the capacitance C_{gs} with temperature are very small, approximately 20% in the whole temperature interval 17–300 K and can be modeled quite accurately with linear functions. The change of the capacitance C_{gd} in a normal active bias state is much smaller, approximately 10% in the whole temperature interval 17–300 K.

Generally in the temperature range 150–400 K the changes of the model parameters with temperature are usually smooth. These temperature variations can be modeled with good accuracy by using linear functions.

$$P(T) = P_0 + A_1 \Delta T \tag{14}$$

where $P(T)$ describes the temperature dependencies of the main parameters. P_0 is the parameter value at room temperature, $\Delta T = T - T_0$ is the difference between ambient and room temperatures. Linear temperature coefficients, A_1, for the main parameters of the measured transistors are presented in Table I. To obtain higher accuracy a quadratic term can be added to the linear equation for temperature variations of the parameters.

Nearly all measured devices showed some unexpected behavior in the temperature range 50–150 K, i.e., a collapse of the I-V characteristics, significant kink effects, strange shapes of the transconductance curves, strange shape of I_{ds} versus V_{ds} dependencies at positive gate voltages, etc. All this made the extraction procedure nearly impossible. At lower temperatures (17–50 K) the transistor characteristics are smoother and more predictable performance has been monitored. To make models

TABLE I
TEMPERATURE COEFFICIENTS FOR MODEL PARAMETERS ($A_1 * 10^3$), T_o = 300 K

	Ipks	Vpks	Vpk0	P1s	P10	λ	α	R_s	C_{gs0}
MGF4317D	-1.3	-2.7	-1.15	0.2	-1.6	-0.2	-1.01	1.3	0.7
MGF1303	-1.18	-0.6	-1.55	0.3	-0.67	-0.27	-0.1	0.7	0.34
NEC32684	-1.23	-2.89	-2.06	0.7	-1.3	-0.36	-0.73	1.44	
FHX15	-0.46	-3.33	-1.45	-1.3	-1.75	-0.4	-0.2	1.08	

TABLE II
MGF4317D: V_{ds} = 2V: 20 K AND 300 K, DEVICE NO. 1

T	Ipks	Vpks	Vpk0	P1s	P10	B	P2	P3	λ	α	C_{gs0}	C_{gd0}	Cds	Rg	Rd	Rs	Rin
K	mA	V	V	1/v	1/v	1/v	$1/V^2$	$1/V^3$	1/v	1/v	fF	fF	fF	Ω	Ω	Ω	Ω
20	53	0.33	0.48	2.5	7.5	4	-0.2	7.8	0.17	3.5	240	35	120	2.3	2.5	1.7	4
300	44	0.30	0.05	2.55	6.1	4	-0.8	3.8	0.15	2.4	280	35	120	2.5	3	1.9	5

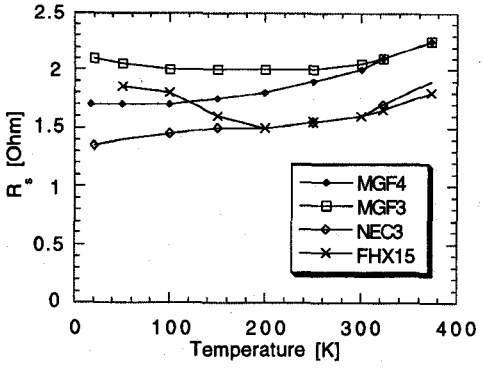

Fig. 13. R_s as function of temperature.

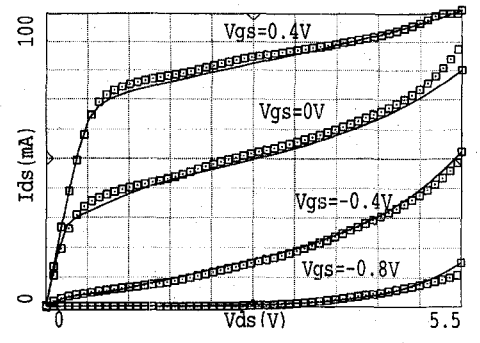

Fig. 15. Drain current I_{ds} as a function of drain voltage V_{ds} for MGF4317D at 300 K. V_{gs} = −0.8, −0.4, 0.0, 0.4 V.

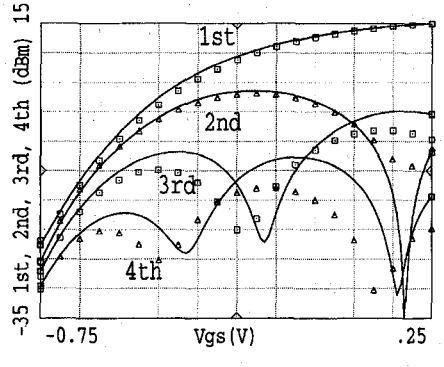

Fig. 14. Power spectrum as function of gate voltage for MGF4317D at 20 K. f_{in} = 2.5 GHz, P_{in} = 0 dBm, V_{ds} = 2 V.

that can describe transistors behavior in the entire temperature range 17–400 K seems to be difficult.

The measured and simulated power spectrum for MGF4317D at 20 K are compared in Fig. 14 [20], where dots show the experimental results and lines the modeled ones. MDS was used for the simulation and the correspondence is good. Device large signal parameter values at 20 K and 300 K are listed in Table II.

For small signal applications the drain current reduction caused by thermal heating effects can be neglected in most cases, but for medium and high power applications the dissipated power P_d is large enough to heat the transistor to temperature T and thus significantly change the model parameters [18]

$$T = \frac{T_0}{\left[1 - \frac{\theta(T_0)P_d}{4T_0}\right]^4} \tag{15}$$

where $\theta(T_0)$ is the thermal impedance at ambient temperature T_0. At small power dissipation and constant temperature distribution in the channel the temperature rise $\Delta T = \theta(T_0)P_d$ can be considered linear. The influence of self heating can be found by interactively solving nonlinear temperature equations at two temperatures, when thermal impedance $\theta(T_0)$, temperature change $\Delta T = T_2 - T_1$ and P_d are given. This process is not straightforward, since the interdependence of the self heating processes and the trap occupancy problem cannot be independently controlled in a simple way. The problem cannot be solved by using the most common software packages available today, such as MDS and Microwave Harmonica. When an approximate linear solution is possible and trapping processes are not influenced by the temperature rise, the change of I_{ds} at dc can be modeled in these programs through different model parameter temperature dependencies and in a

TABLE III
MGF4317D: V_{ds} = 4 V, 300 K, DEVICE No. 2

I_{pks}	V_{pks}	V_{pk0}	P_{1s}	P_{10}	B	P_2	P_3	λ	α_1	α_r	L_{b0}	L_{dl}	L_{gl}	V_{tr}	K_{trg}	K_t
mA	V	V	1/v	1/v	1/v	$1/V^2$	$1/V^3$	1/v	1/v	1/v		1/v	1/v	V	V	1/W
46	0.03	-0.3	2.1	3.0	4	-1.0	1.0	0.15	2.1	0.05	0.016	1.6	0.7	1.9	1	0.25

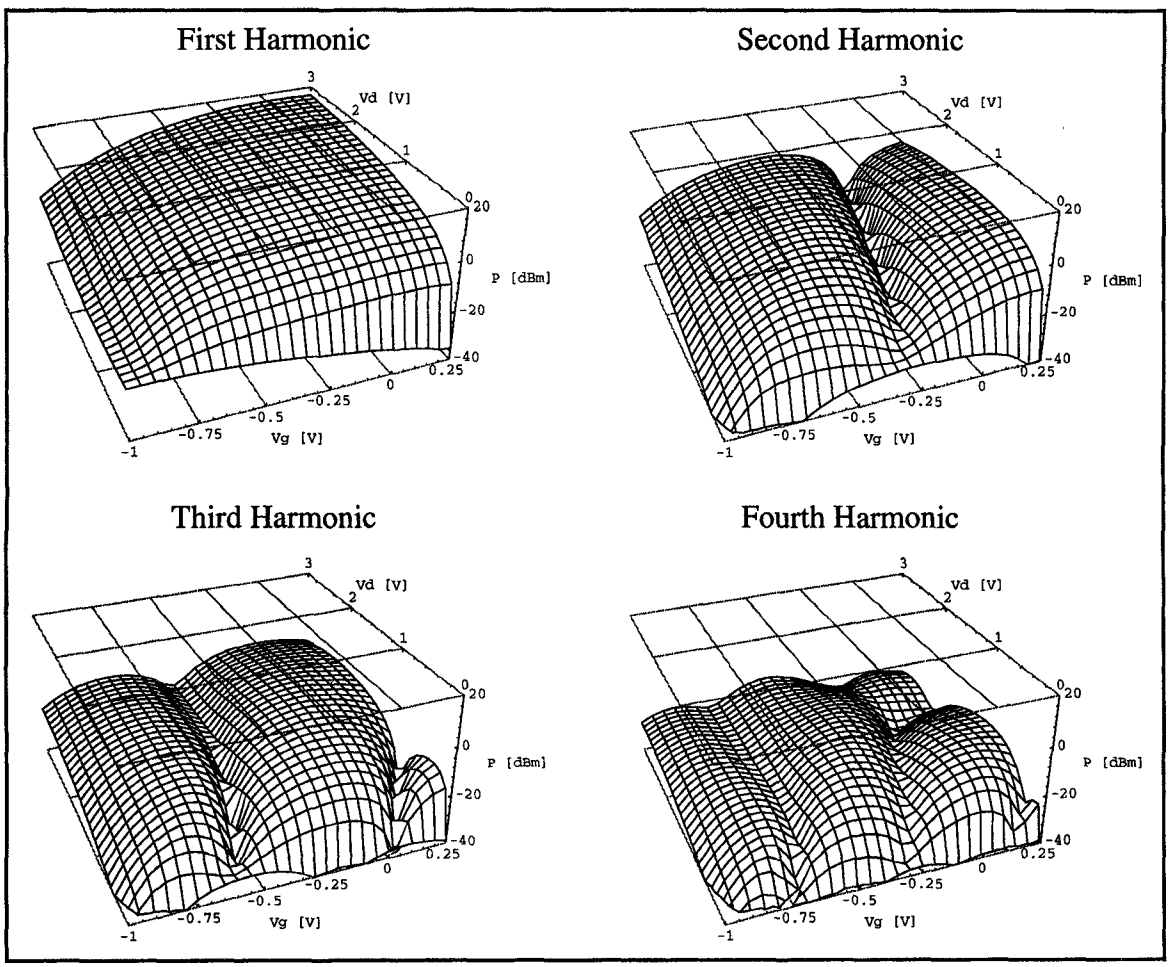

Fig. 16. Measured power spectrum for MGF4317D, P_{in} = 0 dBm.

simpler form this can be expressed as [16]

$$I_{\text{dstem}} = \frac{I_{\text{ds}}}{1 + K_t P_d} \tag{16}$$

where K_t is the thermal constant for the transistor that summarizes the temperature changes of the different large signal model parameters influenced by the temperature rise under the total dissipated power $P_d \approx I_{\text{ds}}(t) \cdot V_{\text{ds}}(t)$. Since the temperature coefficients of the model different parameters are very small (in the order of 10^{-3}), this approximation usually works satisfactorily and can be easily incorporated in a harmonic balance simulator. Using such an approach it is possible to obtain information about the transistor temperature changes due to self heating. A better way to handle this problem is to define a thermal port where the device temperature is the analogous voltage across the thermal port and the dissipated power is the analogous port current. Then an arbitrary thermal circuit can be constructed externally to the device model [23].

VI. SOFT BREAKDOWN MODELING

For many HEMT devices it is possible to monitor an abrupt increase of the drain current well below the breakdown by increasing the drain voltage above some specific threshold V_{tr}. This is especially noticeable at gate voltages close to pinch off. For some devices this drain current increase is rather smooth, while for other it is accompanied by a shift of the gate voltage V_{pk}, at which the maximum transconductance occurs. Since the gate current I_{gs} is much lower than the drain current I_{ds}, the increase is not due to gate breakdown [24]. It can be attributed to the increase of the positive hole charges in the substrate, which widens the channel thickness and leads to an abrupt increase of the drain current. The cause for this effect is not entirely clear but it can be partly explained with the trapping effects phenomena. The breakdown phenomenon is different at dc and RF. The occurrence of RF breakdown is more usual at higher drain voltages than at dc. Soft breakdown

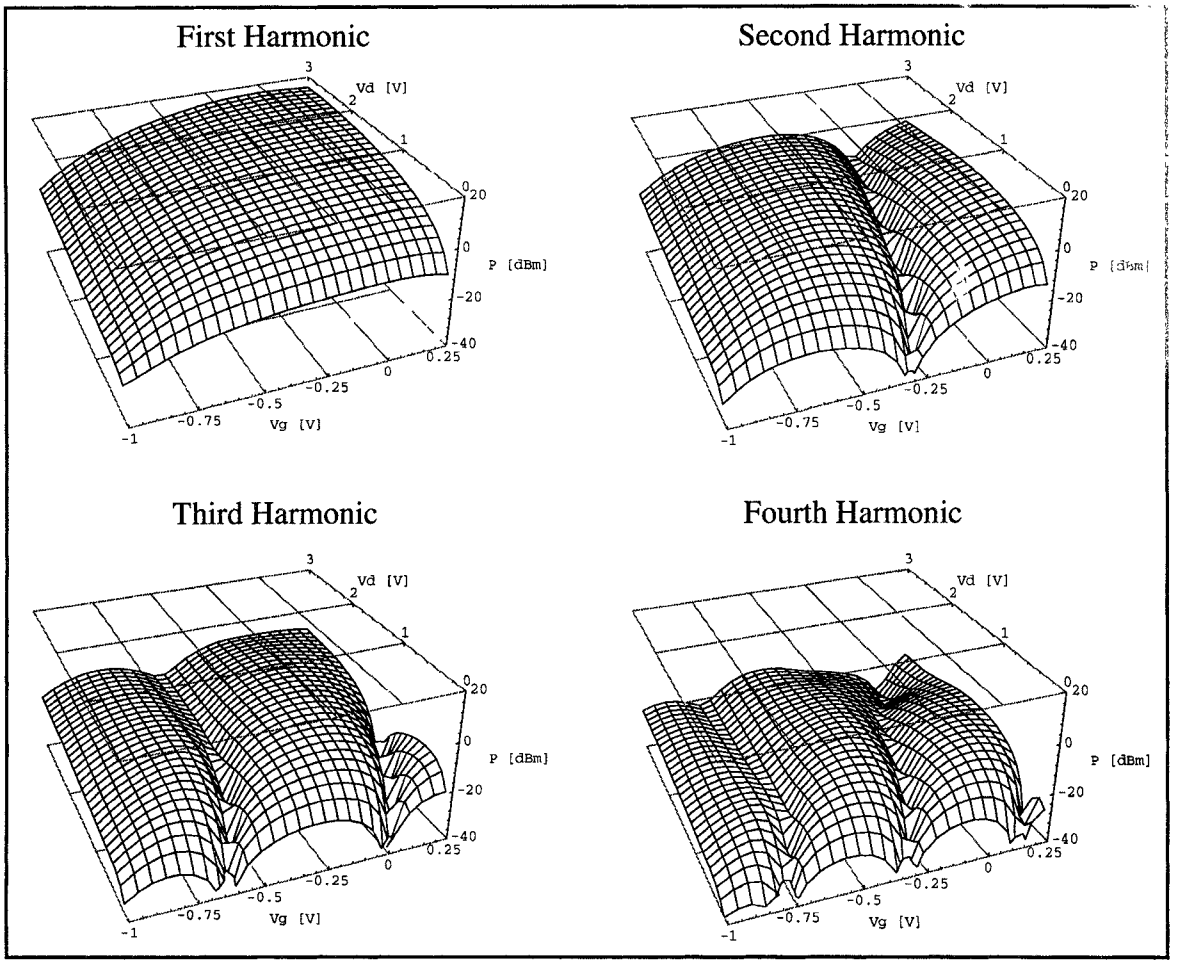

Fig. 17. The Chalmers model, simulation results, $P_{\text{in}} = 0$ dBm.

strongly influences the dc characteristics and output power of the device, therefore the operating point should be carefully selected. Due to the soft breakdown in some devices the increase of the drain voltage leads to the decrease of the output power due. Two approaches for modeling these effects can be found in [16], [25].

In the first approach a combination of gate and drain voltages forms a polynomial dependence of the soft breakdown [16]. By using this procedure it is possible to obtain good correspondence between simulations and measurements. In the second approach a linear combination of the gate and drain voltages forms an exponential dependence of the soft breakdown [25]. Our investigations of many GaAs and InP based devices clearly indicate that at gate voltages close to pinch off this increase of the drain current is very close to the exponential behavior. At gate voltages closer to the normal operating condition of a class A amplifier the power of the exponential function is much lower and the changes of the I_{ds} are more gradual. At high positive gate voltages the soft breakdown effect is usually masked by the thermal heating and the device comes easily to the thermal breakdown. For soft breakdown modeling we therefore consider it preferable to use the exponential approach with some modifications. In our model the drain current equation is extended with a new term L_{sb}

$$I_{\text{ds}} = I_{pk}(1 + \tanh(\Psi))\tanh(\alpha V_{\text{ds}})(1 + \lambda V_{\text{ds}} + L_{sb}) \quad (17)$$

$$L_{sb} = L_{sb0}[\exp(L_{sd1}V_{\text{dgt}} + \cdots) - 1] \quad (18)$$

$$V_{\text{dgt}} = \frac{V_{\text{ds}} - K_{trg}V_{\text{gs}}}{V_{\text{tr}}} \quad (19)$$

$$L_{sd1} = L_{d1}(1 - L_{g1}V_{\text{gs}}) \quad (20)$$

where L_{sb0} and L_{sd1}, are the coefficients matching the drain current dependencies and V_{dgt} is a normalized coefficient that combines the gate and drain voltages. If higher accuracy is needed more terms can be added to (18).

In Fig. 15 modeled and measured results for I_{ds} versus V_{ds} for MGF4317D at 300 K are shown. Equation (7) is used to describe the α dependence of the gate voltage. Soft breakdown and self heating are included in the model (17)–(20). Device parameters are listed in Table III. Measured and modeled PSM for this device are shown in Figs. 16 and 17, respectively. The maximum output power is 18 dBm and the difference between measured and simulated first harmonic is less than 0.4 dB. The global mean error for the higher harmonics is less than 3 dB. Fig. 18(a) and (b), which show cross sections of the global PSM spectrum, visualise this in greater details.

Simulated and experimental PSM as functions of V_{ds} are shown in Fig. 18(b) for the HEMT and Fig. 19 for the MES-

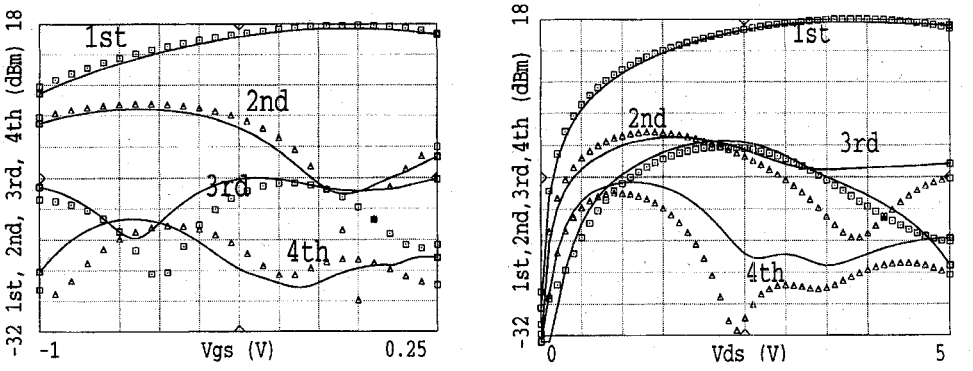

Fig. 18. Power spectrum for HEMT MGF4317D with α dependence and soft-breakdown included. $f_{\text{in}} = 2.5$ GHz, $P_{\text{in}} = 3$ dBm, $T = 300$ K, $\alpha = 0.05 + 2.1 \cdot [1 + \tanh(\psi)]$: (a) Power spectrum as function of gate voltage, $V_{\text{ds}} = 4.0$ V. (b) Power spectrum as function of drain voltage, $V_{\text{gs}} = 0$ V.

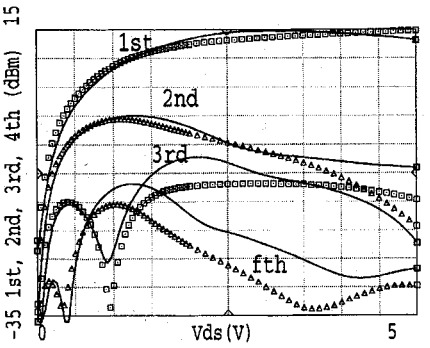

Fig. 19. Power spectrum as function of drain voltage for MESFET MGF1303 with α dependence and soft-breakdown included. $f_{\text{in}} = 2.5$ GHz, $P_{\text{in}} = 3$ dBm, $V_{\text{gs}} = 0.0$ V, $\alpha = 2.9 + 0.3 \cdot [1 + \tanh(\psi)]$.

FET. Similar results were obtained for many MESFET's and HEMT's. These power spectrums show very clearly the influence of the gate voltage dependence on α, especially at low drain voltages. If α dependence is not included in the HEMT model, simulated power at higher harmonics will be wrong at low drain voltages and the picture will be similar to the power spectrum results obtained for the MESFET (Fig. 19). In the power spectrum of the MESFET there is a local maximum at the second harmonic at low drain voltages and dips for the 3rd and 4th harmonics. This can be obtained in the simulation by taking α as a constant. HEMT's, on the other hand, need to be modeled with a gate voltage dependent α. This leads to a power spectrum where the third harmonic increases monotonously at low drain voltages.

If the soft breakdown is not included in the model it is not possible to predict the output power maximum at $V_{\text{ds}} = 4$ V [Fig. 18(b)] and the output power decrease when the drain voltage is further increased. As it is shown in Figs. 18 and 19 the correspondence with the experimental data is quite good especially for the first harmonic.

The difference between the simulated and experimental data for the higher harmonics at high drain voltages can be partially explained by the existence of a "kink" effect in the transistor. This effect has not yet been included in the model. Another reason for the difference is that for simplicity we used only one term (L_{d1}) in the soft breakdown model.

VII. Conclusion

Temperature, dispersion, and soft breakdown effects found in HEMT's and MESFET's were investigated in the temperature range 17–400 K. We have shown that it is possible to extend the Chalmers nonlinear model with the ability to model these effects. A new function for the α parameter has also been added to the model. The model extensions give a good correspondence between measurements and simulations.

Acknowledgment

The authors would like to thank Hewlett-Packard and Compact Software for their donation of high frequency simulation software; E. Kollberg, H. Zirath, P. Starski of CTH, and G. Ericsson of FMV for their strong support of this work; and J. Gerber, G. Ghione, R. Anholt, and G. Vendelin for valuable discussions and suggestions on the subject of the paper.

References

[1] W. Curtice, "A MESFET model for use in the design of GaAs integrated circuit," *IEEE Trans. Microwave Theory Tech.*, vol. 28, no. 5, pp. 448–455, 1980.

[2] A. Materka and T. Kacprzak, "Computer calculation of large-signal GaAs FET amplifiers characteristics," *IEEE Trans. Microwave Theory Tech.*, vol. 33, no. 2, pp. 129–135, 1985.

[3] I. Angelov, H. Zirath, and N. Rorsman, "A new empirical model for HEMT and MESFET devices," *IEEE Trans. Microwave Theory Tech.*, vol. 40, no. 12, pp. 2258–2266, 1992.

[4] P. Ladbrooke and S. Blight, "Low-field low-frequency dispersion of transconductance in GaAs MESFET's with implication for other rate-dependent anomalies," *IEEE Trans. Electron Devices*, vol. 35, no. 3, p. 257, Mar. 1988.

[5] M. Paggi, P. Williams, and J. Borrego, "Nonlinear GaAs MESFET modeling using pulsed gate measurements," *IEEE Trans. Microwave Theory Tech.*, vol. 36, no. 12, pp. 1593–1597, Dec. 1988.

[6] J. P. Teyssier, M. Campovecchio, C. Sommet, J. Portilla, and R. Quere, "A pulsed S-parameter measurement set-up for the nonlinear characterization of FET's and bipolar transistors," in *Proc. 23rd EuMC*, Madrid, 1993, p. 489.

[7] J. Reynoso-Hernandez and J. Graffeuil, "Output conductance frequency dispersion and low-frequency noise in HEMT's and MESFET's," *IEEE Trans. Microwave Theory Tech.*, vol. 37, no. 9, pp. 1478–1481, Sept. 1989.

[8] C. Camacho-Penalosa and C. Aitchison, "Modeling frequency dependence of output impedance of a microwave MESFET at low frequencies," *Electronics Lett.*, vol. 21, no. 12, pp. 528–529, June 1985.

[9] R. Anholt and S. Swirhun, "Experimental investigation of the temperature dependence of GaAs FET equivalent circuits," *IEEE Trans. Electron Devices*, vol. 39, no. 9, p. 2029, Sept. 1992.
[10] Y. J. Chan and M. Y. Yang, "Device linearity imptovement by $Al_{0.3}Ga_{0.7}As/In_{0.2}Ga_{0.8}As$ heterostructure doped-chanel FET's," *IEEE Electron Device Lett.*, vol. 16, no. 1, pp. 33–35, Jan. 1995.
[11] I. Angelov, H. Zirath, and N. Rorsman, "Validation of a nonlinear HEMT model by power spectrum characteristics," in *IEEE Microwave Theory Tech. Dig.*, 1994, pp. 1571–1574.
[12] L. Bengtsson, M. Garcia, and I. Angelov, "An extraction program for nonlinear transistor model parameters for HEMT's and MESFET's," *Microwave J.*, vol. 38, no. 1, pp. 146–153, Jan. 1994.
[13] *Microwave Harmonica*, SCOUT, Compact Software Inc.
[14] T. Brazil, "A universal large-signal equivalent circuit model for the GaAs MESFET," in *Proc. 21st EuMC*, 1991, pp. 921–926.
[15] C. Rauscher and H. A. Willing, "Simulation of nonlinear microwave FET performance using a quasistatic model," *IEEE Trans. Microwave Theory Tech.*, vol. MTT-27, no. 10, pp. 834–840, Oct. 1979.
[16] M. Pirola, G. Ghione, J. M. Dortu, and J. Muller, "A large-signal model for medium power pseudomorphic HEMT's for K-Ka band applications," *IEEE MTT-S European Topical Congress Technologies Wireless Applications*, 1994, pp. 43–48.
[17] G. Kompa, "Modeling of dispersive microwave FET devices using a quasistatic approach," *Int. J. Microwave and Millimeter-Wave Computer-Aided Engineering*, vol. 5, no. 3, 173–194, 1995.
[18] R. Anholt, *Electrical and Thermal Characterization of MESFET's, HEMT's, and HBTs*. Norwood, MA: Artech House, 1995.
[19] P. Ladbrooke, A. J. Hill, and J. P. Bridge, "Negative R_s and R_d in GaAs FET and HEMT equivalent circuits," *Electronics Lett.*, vol. 26, no. 10, p. 680, May 1990.
[20] P. Roblin *et al.*, "Nonlinear parasitics in MODFET's and MODFET IV characteristics," *IEEE Trans. Electron Devices*, vol. 35, no. 8, pp. 1207–1214, Aug 1988.
[21] H. Fukui, "Thermal resistance of GaAs FET," in *Proc. IEDM'80*, 1980, pp. 118–121.
[22] J. Bandler, Q. Zhang, S. Ye, and S. Chen, "Efficient large-signal FET parameter extraction using harmonics," *IEEE Trans. Microwave Theory Tech.*, vol. 37, no. 12, pp. 2099–2108, Dec. 1989.
[23] J. Gerber, R. Anholt, R. Tayrani, and J. Pence, "A self-heating HBT model for harmonic-balans simulators with parameter extraction," *Asia-Pacific Microwave Conf.*, 1994, pp. 1029–1032.
[24] R. J. Trew, "MESFET models for microwave CAD applications," *Microwave and Millimeter-Wave CAE*, vol. 1, no. 2, pp. 143–158, Apr. 1991.
[25] J. P. Teyssier, L. P. Viaud, and R. Quere, "A new nonlinear I(V) model for FET devices including breakdown effects," *IEEE Microwave Guided Wave Lett.*, vol. 4, no. 4, pp. 104–107, Apr. 1994.

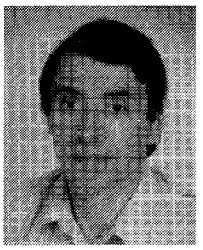

Iltcho Angelov (M'89) received the M.Sc. degree in electronics in 1969 and the Ph.D. degree in physics and mathematics in 1973.

Since 1976 he has worked with microwave oscillators, low noise transistor amplifiers and receivers, including criogenically cooled amplifiers. Recently his research activity is in the field of HEMT nonlinear modeling and development of millimeter wave HEMT mixers and multipliers.

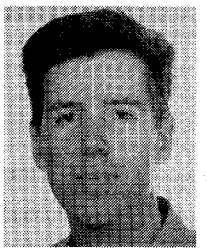

Lars Bengtsson (S'94) received the M.Sc. degree in electrical engineering from Chalmers University of Technology in 1993. Since then, he has been working toward the Ph.D degree.

His research activity is in the field of HEMT, MESFET, and HBT nonlinear modeling.

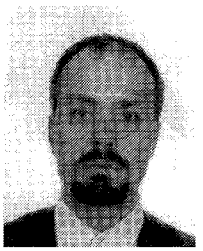

Mikael Garcia (S'93) received the M.Sc. degree in electrical engineering from Chalmers University of Technology in 1992. Currently he is working toward the Ph.D. degree.

His research interests are in the area of HFET and MESFET modeling.